

High-Dynamic-Range Laser Amplitude and Phase Noise Measurement Techniques

Ryan P. Scott, *Student Member, IEEE*, Carsten Langrock, and Brian H. Kolner, *Member, IEEE*

Invited Paper

Abstract—We describe techniques for making sensitive and high-dynamic-range measurements of laser amplitude and envelope phase noise (timing jitter) in the frequency domain at the shot-noise limit. Examples of amplitude noise measurements on continuous-wave argon-ion and diode-pumped solid-state lasers used for pumping a femtosecond Ti:sapphire laser are presented. Amplitude and phase noise measurements for the Ti:sapphire laser are also presented, showing correlation between pump laser amplitude modulation (AM) spectra and the resulting AM and phase noise. Characteristics of the measurement system components are discussed, along with examples of the impact these have on achieving reliable high-dynamic-range measurement capability.

Index Terms—Amplitude modulation (AM) noise, mode-locked lasers, noise measurement, phase-locked loops, phase noise, p-i-n photodiodes, shot noise, timing jitter.

I. INTRODUCTION

THE MEASUREMENT of laser noise has long been an important part of laser science, yet good techniques for noise characterization have not enjoyed widespread practice. Modern diode-pumped solid-state laser sources are demonstrating extraordinary noise performance, and accurately characterizing the noise is challenging. It is no longer sufficient to estimate the standard deviation of the average photocurrent displayed on an oscilloscope. Moreover, mode-locked femtosecond lasers combine contributions from timing jitter (phase noise) and pulse energy fluctuations to that of the amplitude noise. The high peak-to-average ratio of detected photocurrent adds a further element to the long list of possible sources of error in these types of measurements.

It has been our experience that numerous pitfalls plague the process of laser noise characterization. However, with care and attention to many subtle issues of extraneous noise contributions, accurate and high-dynamic-range laser noise measurements are possible. Much of our work builds on

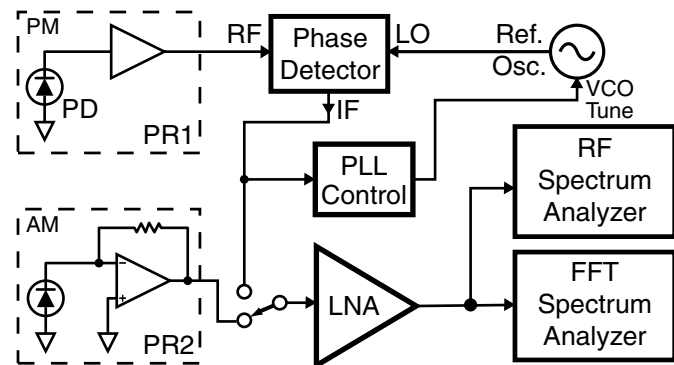


Fig. 1. Typical measurement setup for spectral analysis of laser noise. LNA: low noise amplifier; PD: photodiode; LO: local oscillator port; RF: radio frequency port; PR1: phase noise photoreceiver; PR2: amplitude noise photoreceiver.

the pioneering efforts at standards laboratories and test and measurement instrument manufacturers worldwide who paved the way by making similar measurements on precision clocks and oscillators. Most of their work is well documented and readily available. Though developed for electronic sources, the basic tools, techniques, and nomenclature are adaptable to laser science. The reader will profit immensely from familiarity with this literature [1]–[5].

In this paper, we present a theoretical framework for describing noise and techniques that we have developed for making reliable measurements of laser amplitude and phase noise using fast Fourier transform (FFT) and radio-frequency (RF) spectrum analyzers (Fig. 1). Although there are many reports of laser amplitude and phase-noise measurements in the literature [6]–[23], we feel that there is room for a more comprehensive treatment of the “art” of laser-noise measurement. Essential to making these types of measurements is an understanding of the influence of extraneous noise sources within the local environment and from associated electronic components as well as the role of optimum photoreceiver design. The latter is especially significant when trying to make low-level noise measurements in the presence of high background signals. We discuss the principles of this type of photoreceiver design, which are distinctly different from photoreceivers optimized for photon counting or high-speed communications. We then show examples of applications to diode-pumped solid-state laser, argon-ion laser, and mode-locked Ti:sapphire laser noise. The

Manuscript received April 27, 2001; revised August 23, 2001. This work was supported by the David and Lucile Packard Foundation.

R. P. Scott is with the Electrical Engineering Department, University of California, Los Angeles, CA 90095 USA.

C. Langrock is with the Department of Electrical Engineering, Stanford University, Stanford, CA 94305 USA.

B. H. Kolner is with the Department of Applied Science, University of California, Davis, CA 95616 USA.

Publisher Item Identifier S 1077-260X(01)09937-3.

characterization of both amplitude and envelope phase noise (timing jitter) is presented with shot-noise-limited sensitivity over most of the range from 1 Hz to 40 MHz.

II. THE NATURE OF THE SIGNAL

A. Noise in the Frequency Domain

The random noise associated with amplitude and phase variations of a periodic signal are most easily studied in the frequency domain. There are several reasons for this. First, experimental techniques exist to readily separate the effects of amplitude and phase modulation. Second, narrow-band spectrum analyzers dramatically reduce the effects of measurement system noise contributions, thus extending the measurement dynamic range. Third, the spectra of amplitude and phase fluctuations contain a wealth of information about the sources of the noise and therefore hints for their reduction. For example, a broad, continuous peaked spectrum may contain the signature of relaxation oscillation [24]. Discrete spectral lines at multiples of 60 Hz or several tens or hundreds of kilohertz are usually associated with power supplies. Cooling fan and other vibrationally or electromagnetically induced discrete spurious lines (spurs) may also be visible and may or may not actually be modulation on the beam. If not, the spectrum analyzers are good tools for hunting down these sources of interference.

Direct measurement of noise sideband amplitude of a mode-locked laser at the pulse repetition frequency or one of its harmonics [6] is of very limited utility because of limitations on the dynamic range of spectrum analyzers and the bandwidth of the filters employed when scanning over large frequency ranges. Although a popular technique for characterizing phase noise, this approach suffers from serious inaccuracy at high harmonics where the linear approximation to the phase modulation process breaks down. For measuring phase noise, demodulation to baseband allows the use of much higher resolution bandwidths and simultaneously removes the large background carrier, giving an effective improvement in dynamic range. Measuring amplitude noise is inherently a baseband process, although it can be done, with limitations, by demodulating the carrier.

Suppose we observe the spectrum of a train of current pulses from a photodiode illuminated by mode-locked laser pulses [Fig. 2(a)]. This is the simplest experimental setup and the starting point for understanding laser noise spectra. Looking closely at any one of the prominent spectral features [Fig. 2(b)], we see that there is a major component at multiples of the pulse repetition frequency along with a pedestal of noise in the sidebands that falls away toward the noise floor of the system. There are really only two degrees of freedom that can be characterized in this spectral component: the instantaneous amplitude and phase perturbations of the carrier. The main task in this measurement is to deduce from the noise sidebands the magnitudes of the amplitude and phase perturbations in both absolute terms and in relation to the carrier. The majority of this paper is devoted to the accurate characterization of the statistical averages of these quantities at frequencies adjacent to the carrier. How the magnitudes of these perturbations amongst

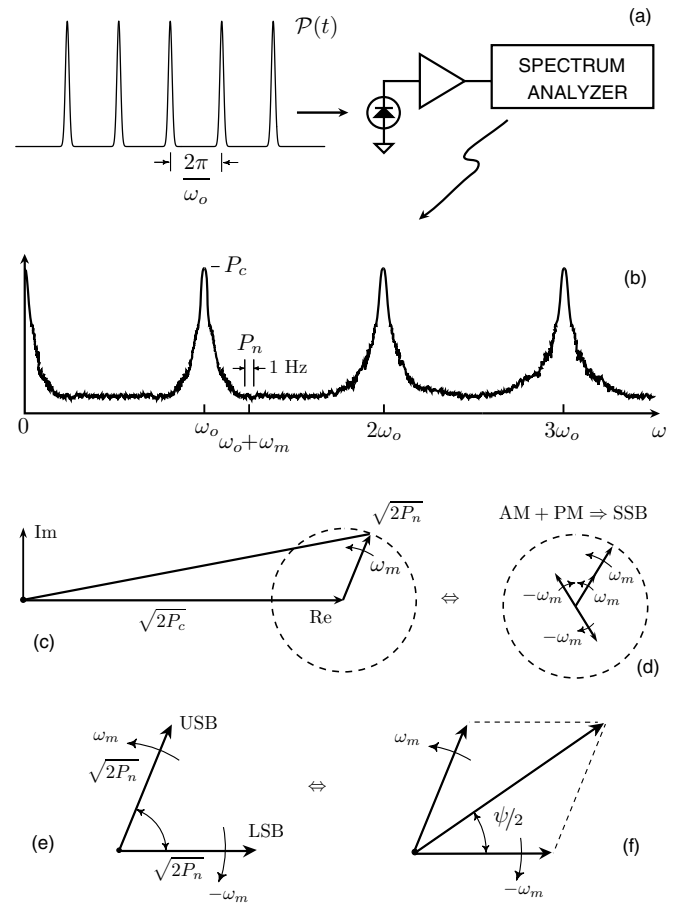


Fig. 2. Measurement of mode-locked laser noise in the frequency domain. (a) Laser pulse train $\mathcal{P}(t)$ is converted to current pulses $i(t)$ in a photodiode, which are then sent to a spectrum analyzer. (b) Spectra of lowest Fourier components. P_c : carrier power; P_n : noise spectral density (W/Hz). (c) Phasor representation of carrier plus single-sideband noise. Phasor amplitudes are peak voltages or currents in a 1- Ω resistor. (d) Decomposition of single-sideband noise into AM and PM components, each carrying power $P_n/4$. (e) Double sideband noise phasors in the rotating reference frame of the carrier with an arbitrary phase offset ψ shown at $\omega_m t = 0$. (f) Superposition of upper and lower sideband phasors results in stationary (with respect to carrier) noise component with magnitude oscillating at ω_m and projection on real and imaginary parts of the carrier depending on phase angle $\psi/2$.

all harmonics relate to overall pulse train dynamics such as pulse width or pulse energy modulation has been treated extensively elsewhere [25]–[28].

Since a spectrum analyzer is a tuned narrow-band root-mean-square (rms) voltmeter, we can consider the sideband amplitude as representing the total noise power filling the analyzer's receiver bandwidth B . For the purposes of this model, we assume that the source of the noise is a random process and can be modeled in the narrow-band approximation as having uniform (white) spectral density with units of $V/\sqrt{\text{Hz}}$ or $A/\sqrt{\text{Hz}}$. When white noise is passed through a narrow-band filter and observed on an oscilloscope, for a time of the order of the inverse of the filter bandwidth, the waveform will appear approximately sinusoidal. Thus, it will be convenient to describe the noise in the sidebands as coherent modulation, where it is understood that this applies only to the extent of times commensurate with $1/B$. The results of this analysis will then also apply to the long-term mean-squared values of the spectral densities.

B. Review of Modulation Theory

A double-sideband large-carrier AM current signal with carrier power P_c (into 1 Ω) can be written as

$$\begin{aligned} i_{AM}(t) &= \sqrt{2P_c}[1 + m \cos \omega_m t] \cos \omega_0 t \\ &= \sqrt{2P_c} \operatorname{Re} \left\{ e^{i\omega_0 t} + \frac{m}{2} \left(e^{i(\omega_0 + \omega_m)t} + e^{i(\omega_0 - \omega_m)t} \right) \right\} \\ &= \sqrt{2P_c} \operatorname{Re} \left\{ e^{i\omega_0 t} \left[1 + \frac{m}{2} (e^{i\omega_m t} + e^{-i\omega_m t}) \right] \right\} \quad (1) \end{aligned}$$

where

- ω_0 carrier frequency;
- ω_m modulation frequency;
- m modulation index.

The single-sideband (SSB) AM/carrier power ratio is therefore

$$\frac{P_{SSB_AM}}{P_c} = \frac{m^2}{4}. \quad (2)$$

A sinusoidal carrier undergoing phase modulation (PM) can be written

$$\begin{aligned} i_{PM}(t) &= \sqrt{2P_c} \cos(\omega_0 t + \beta \sin \omega_m t) \\ &= \sqrt{2P_c} \operatorname{Re} \{ e^{i\omega_0 t} e^{i\beta \sin \omega_m t} \} \\ &= \sqrt{2P_c} \operatorname{Re} \left\{ e^{i\omega_0 t} \sum_{n=-\infty}^{\infty} J_n(\beta) e^{in\omega_m t} \right\} \quad (3) \end{aligned}$$

where the J_n are Bessel functions of the first kind and β is the peak phase deviation or phase modulation index. We can simplify this result using the small modulation index approximation

$$J_n(\beta) \approx \begin{cases} 1 & n = 0 \\ \pm\beta/2 & n = \pm 1 \\ 0 & |n| > 1 \end{cases} \quad \beta \ll 1 \quad (4)$$

and the symmetry property of the Bessel functions; $J_{-1}(\beta) = -J_1(\beta)$, so that

$$\begin{aligned} i_{PM}(t) &\approx \sqrt{2P_c} \operatorname{Re} \left\{ e^{i\omega_0 t} + \frac{\beta}{2} \left[e^{i(\omega_0 + \omega_m)t} - e^{i(\omega_0 - \omega_m)t} \right] \right\} \\ &= \sqrt{2P_c} \operatorname{Re} \left\{ e^{i\omega_0 t} \left[1 + \frac{\beta}{2} (e^{i\omega_m t} - e^{-i\omega_m t}) \right] \right\}. \quad (5) \end{aligned}$$

The single-sideband PM/carrier power ratio for phase modulation is seen to be

$$\frac{P_{SSB_PM}}{P_c} = \frac{\beta^2}{4}. \quad (6)$$

C. Decomposition of Single-Sideband Noise

The last of equations (1) and (5) display complex phasor amplitudes on the carrier $e^{i\omega_0 t}$ and can serve as a basis for decomposing an SSB noise component. For example, consider a 1-Hz slice of the noise spectrum adjacent to the carrier in Fig. 2(b). The power in the carrier is P_c at frequency ω_0 . At the offset frequency $\omega_0 + \omega_m$, there is pure noise with spectral density P_n W/Hz. For times on the order of 1 s, the signal within this slice is approximately sinusoidal, and when combined with the carrier can be thought of as a complex phasor rotating at angular frequency $\omega_0 + \omega_m$ connected to the end of the carrier as shown in Fig. 2(c). The total current for the carrier plus SSB noise is

$$i(t) = \operatorname{Re} \left\{ \sqrt{2P_c} e^{i\omega_0 t} + \sqrt{2P_n} e^{i(\omega_0 + \omega_m)t} \right\} \quad (7)$$

$$= \operatorname{Re} \left\{ e^{i\omega_0 t} \left(\sqrt{2P_c} + \sqrt{2P_n} e^{i\omega_m t} \right) \right\}. \quad (8)$$

It is intuitively clear from the figure that the single-sideband noise contributes equally to amplitude and phase modulation of the carrier. We can show this analytically by expanding the sideband term in (8)

$$\begin{aligned} &\sqrt{2P_n} e^{i\omega_m t} \\ &= \sqrt{2P_n} (\cos \omega_m t + i \sin \omega_m t) \quad (9) \end{aligned}$$

$$= \sqrt{\frac{P_n}{2}} \left[\underbrace{\left(e^{i\omega_m t} + e^{-i\omega_m t} \right)}_{AM} + \underbrace{\left(e^{i\omega_m t} - e^{-i\omega_m t} \right)}_{PM} \right]. \quad (10)$$

Comparing (10) with (1) and (5), we see that an SSB pure noise signal can be decomposed into four phasors: two that comprise pure AM and two that comprise pure PM. The amplitude of each phasor is half that of the original SSB noise phasor. Thus the power in each of the four sidebands is $P_n/4$, or P_n (dB) $- 6$ dB. Half the power in SSB noise resides in AM (in phase with the carrier) and half resides in PM (in quadrature with the carrier). Fig. 2(d) displays this decomposition. Note that the lower sideband terms are exactly 180° out of phase and thus cancel while the upper sideband terms are in phase and add coherently.

Real carriers usually have unequal contributions from AM and PM. How can this be, in light of the previous discussion? The answer lies in the contribution from SSB noise on the other side of the carrier (lower sideband) at the same offset frequency and its phase relationship to the upper sideband noise. Consider the superposition of upper and lower sideband noise terms with long-term average rms values $\sqrt{2P_n}$, as shown in Fig. 2(e). In the reference frame of the carrier, the upper sideband (USB) and lower sideband (LSB) phasors are spinning at $\pm\omega_m t$, respectively. However, the relative phase offset determines whether the superposition will create pure AM, pure PM, or a mix. [In Fig. 2(e), the phase offset is shown as ψ at time $t = 0$]. Let us calculate the total double sideband (DSB) signal by combining both terms. In complex form

$$i_{DSB}(t) = \sqrt{2P_n} \left[e^{i((\omega_0 + \omega_m)t + \psi)} + e^{i(\omega_0 - \omega_m)t} \right]. \quad (11)$$

Adding the real and imaginary parts separately and using a trigonometric identity, we can rewrite this as

$$\begin{aligned} i_{DSB}(t) &= \sqrt{2P_n} [\cos(\omega_0 t + \psi/2) \cos(\omega_m t + \psi/2) \\ &\quad + i \sin(\omega_0 t + \psi/2) \cos(\omega_m t + \psi/2)] \quad (12) \\ &= 2\sqrt{2P_n} \cos(\omega_m t + \psi/2) e^{i(\omega_0 t + \psi/2)}. \quad (13) \end{aligned}$$

The phasor amplitude coefficient is seen to be stationary in the rotating frame of the carrier, has a phase angle of $\psi/2$, and oscillates in magnitude at the offset frequency ω_m [See Fig. 2(f)]. Thus the phase angle ψ determines the relative amount of phase versus amplitude noise. Note that we are still dealing with a random process. During any particular second, ψ may take on any value, but the long-term average value gives us the average contribution of AM and PM noise.

D. Separation and Measurement of AM and PM Noise

The usual procedure for measuring the characteristics of the amplitude and phase perturbations on the carrier is to downconvert the whole spectrum about the carrier to baseband in a homodyne arrangement. The resultant spectrum, from audio through the RF range, is measured with FFT and RF spectrum analyzers.

The downconversion process takes place in a mixer, which produces an output proportional to the product of the two inputs. In our case, the input or “RF” port is fed with the signal to be analyzed, while the local oscillator (LO) port is driven with a pure sinusoid at frequency ω_0 and an adjustable phase θ . Fixing the phase between the RF and LO signals is essential to separating the AM from the PM. In calculating the product at the mixer output, we must always be careful to use only real quantities; otherwise certain mixing products will be lost. At the mixer output (the “intermediate frequency” or IF port), we have

$$i_{\text{IF}}(t) = i_{\text{LO}}(t)i_{\text{RF}}(t) \quad (14)$$

$$= \sqrt{2P_{\text{LO}}} \cos(\omega_0 t + \theta) \left[\sqrt{2P_c} \cos \omega_0 t + 2\sqrt{2P_n} \times \cos(\omega_m t + \psi/2) \cos(\omega_0 t + \psi/2) \right]. \quad (15)$$

After a little algebra and low-pass filtering to isolate the baseband components, this becomes

$$i_{\text{IF}}(t) = \sqrt{P_{\text{LO}}P_c} \cos \theta + 2\sqrt{P_{\text{LO}}P_n} \cos(\omega_m t + \psi/2) \times \left[\underbrace{\cos \theta \cos \psi/2}_{\text{AM}} + \underbrace{\sin \theta \sin \psi/2}_{\text{PM}} \right]. \quad (16)$$

From Fig. 2(f), we see that $\cos \psi/2$ is the projection of the in-phase, or AM component of the noise, while $\sin \psi/2$ is in quadrature and gives the PM component. Thus, when the local oscillator phase $\theta = 0$, the mixer output is composed of a dc term and the AM component only. When $\theta = \pi/2$, the mixer output is only composed of the PM component, demodulated as a baseband signal. The fact that the dc component is zero and varies linearly through the zero point is handy for controlling a phase-locked loop that can servo the local oscillator to the signal being studied. When the local oscillator is driven in phase quadrature with the incoming RF signal, the mixer functions as a phase detector with an output voltage that is linearly proportional to the phase difference between the LO and RF ports for small phase modulation index.

For measuring the AM noise, a separate mixer could be used with the LO port fed from the same local oscillator as the phase detector but with a 90° phase shift network. Alternatively, a square law device such as a diode and low-pass filter could be used to envelope detect the AM component. This approach is commonly used to detect modulation on RF and microwave carriers, but the dynamic range is limited by saturation at the high end and by threshold effects at the low end [29]. We choose instead to take advantage of the fact that the signal from the photodiode, as a train of pulses, has the AM modulation spectrum common to all harmonics, even at baseband. Thus, simply measuring the spectrum of the photocurrent at baseband gives the AM noise spectrum with no PM noise present.

E. Definitions of Phase Instability

Since our measurements are of noise spectral densities, we must have a common set of spectra with which we can compare different sources [1], [2]. Suppose the output voltage of a sinusoidal oscillator is described by

$$v(t) = V_0 \sin(2\pi\nu_0 t + \phi(t)). \quad (17)$$

Here, all of the phase instability is contained in the function $\phi(t)$, which is a random process, while the constant ν_0 is a nominal carrier frequency. The mean-squared spectrum of $\phi(t)$ is called the phase spectral density $S_\phi(f)$ with units of rad^2/Hz . They are related by Parseval’s theorem

$$\overline{\phi^2(t)} = \lim_{T \rightarrow \infty} \frac{1}{T} \int_{-T/2}^{T/2} |\phi(t)|^2 dt = \int_{-\infty}^{\infty} S_\phi(f) df. \quad (18)$$

Now, suppose the oscillator signal (17) is fed into the RF port of a mixer and the LO port is driven in quadrature with a voltage $v_{\text{LO}}(t) = V_{\text{LO}} \cos 2\pi\nu_0 t$. The output voltage after low-pass filtering is

$$v_{\text{IF}}(t) = \frac{\alpha}{2} V_{\text{LO}} V_0 \sin \phi(t) \approx \frac{\alpha}{2} V_{\text{LO}} V_0 \phi(t) \quad (19)$$

where α is the mixer conversion constant. Thus, for small peak phase deviations, the output of the mixer is linearly proportional to the phase modulation. Since $\phi(t)$ is a random process, we can only deal with statistical quantities and compute, for example, the mean-squared voltage

$$\overline{v_{\text{IF}}^2(t)} = \left[\frac{\alpha V_{\text{LO}} V_0}{2} \right]^2 \overline{\phi^2(t)}. \quad (20)$$

Taking the square root of both sides leads to the definition of the phase detector constant K_ϕ

$$\sqrt{\overline{v_{\text{IF}}^2(t)}} = \frac{\alpha V_{\text{LO}} V_0}{2} \sqrt{\overline{\phi^2(t)}} = K_\phi \sqrt{\overline{\phi^2(t)}} \quad (21)$$

or

$$K_\phi \equiv \frac{\sqrt{\overline{v_{\text{IF}}^2(t)}}}{\sqrt{\overline{\phi^2(t)}}} \quad \text{V/rad}. \quad (22)$$

Although we have developed the concept of K_ϕ for the random phase modulation process $\phi(t)$, it is entirely valid for deterministic signals and holds for instantaneous as well as time-averaged quantities. This allows us to readily measure K_ϕ using a pure sinusoid in place of $\phi(t)$.

Equation (21) suggests that we might choose to define $K_\phi = \alpha V_{\text{LO}} V_0 / 2$, but this is true only for the mixer implementation of the phase detector (other types exist). Equation (22) is general and applies to any phase detector type.

Using a phase detector that converts instantaneous phase deviations into a voltage through a phase detector constant K_ϕ (V/rad), a spectrum analyzer measures the rms voltage spectral density V_ϕ (V/ $\sqrt{\text{Hz}}$) at some offset frequency f , and we compute $S_\phi(f)$ according to

$$S_\phi(f) = \left[\frac{V_\phi(f)}{K_\phi} \right]^2 \quad \text{rad}^2/\text{Hz}. \quad (23)$$

Although we actually measure $S_\phi(f)$ with a phase detector, we often represent the phase noise in terms of the SSB PM noise spectrum adjacent to the carrier. This is the spectrum that results when $S_\phi(f)$ phase modulates the carrier. It is the spectrum that would be measured with a spectrum analyzer tuned to the noise sideband on one side of the carrier if that noise sideband were composed only of phase noise. The representation that is used for this spectral density is denoted $\mathcal{L}(f)$, and its units are dBc/Hz or dB with respect to the power in the carrier. Originally, $\mathcal{L}(f)$ was defined as the ratio of SSB PM noise density to the total signal power, but when the total sideband power is

small compared to the carrier, it is valid and common practice to define $\mathcal{L}(f) = P_n(f)/P_c$.

$\mathcal{L}(f)$ can be directly related to the measured spectrum $S_\phi(f)$ as follows [30]: let $\phi(t)$ be modeled as the narrow-band noise process $\phi(t) = \beta \sin 2\pi f_m t$. The mean-squared phase deviation is $S_\phi(f_m) = \beta^2/2$. Now, imagine this noise process phase modulates the carrier. In the small modulation approximation ($J_1(\beta) \approx \beta/2$), the SSB noise/carrier power ratio is [from (6)] $\mathcal{L}(f_m) = \beta^2/4$. Thus

$$\mathcal{L}(f) = S_\phi(f)/2. \quad (24)$$

So, we merely subtract 3 dB from $S_\phi(f)$ to arrive at $\mathcal{L}(f)$. Provided that the mean-squared phase deviation is small enough ($\ll 1$ rad) so that the linear approximation to the Bessel functions holds, this is valid and it is the spectrum that would be measured with an ideal narrow-band receiver tuned to one side of the carrier. However there are severe demands on filter performance and dynamic range when directly measuring noise sidebands adjacent to a carrier; the phase detector method is vastly superior.

The use of $\mathcal{L}(f)$ as a representation of phase instability has gained wide acceptance. In order to avoid erroneous use of the function when the small modulation index approximation is violated, the IEEE, in Standard 1139-1988, has simply made the following definition: $\mathcal{L}(f) \equiv S_\phi(f)/2$ [31].

III. DYNAMIC RANGE REQUIREMENTS

Very small amplitude fluctuations in a laser source can only be detected when they are stronger than the shot noise accompanying the light (in conventional classical measurement systems). These amplitude fluctuations scale linearly with the optical power while the shot noise goes as the square root. Furthermore, the maximum extraneous noise that can appear on the laser beam is approximately equal to the average laser power. Thus, any system created to reliably characterize laser noise must be capable of handling a large dynamic range with the low end of this range set by the shot noise and the high end set by the average photocurrent. To see what kind of dynamic range is ultimately required (or attainable) in a measurement system, let us simply calculate the shot-noise limited dynamic range inherent in a continuous-wave (CW) laser beam, which produces an average photocurrent $i_0 = \mathcal{R}\mathcal{P}_0$, where \mathcal{R} is the photodetector responsivity and \mathcal{P}_0 is the incident optical power. The fractional rms fluctuation produced by the shot noise is

$$\frac{\Delta i_{\text{rms}}}{i_0} = \frac{\sqrt{2qi_0B}}{i_0} = \sqrt{\frac{2qB}{i_0}} = 5.66 \times 10^{-10} \sqrt{\frac{B}{i_0}} \quad (25)$$

where q is the electron charge and B is the receiver bandwidth. The dynamic range or signal/shot-noise power is thus

$$\text{DR} = \left[\frac{i_0}{\sqrt{2qi_0B}} \right]^2 = \frac{i_0}{2qB} \quad (26)$$

which in decibels normalized to a 1 Hz bandwidth is

$$\text{DR}(\text{dB}) = 155 + 10 \log_{10} [i_0(\text{mA})] \quad \text{dB/Hz}. \quad (27)$$

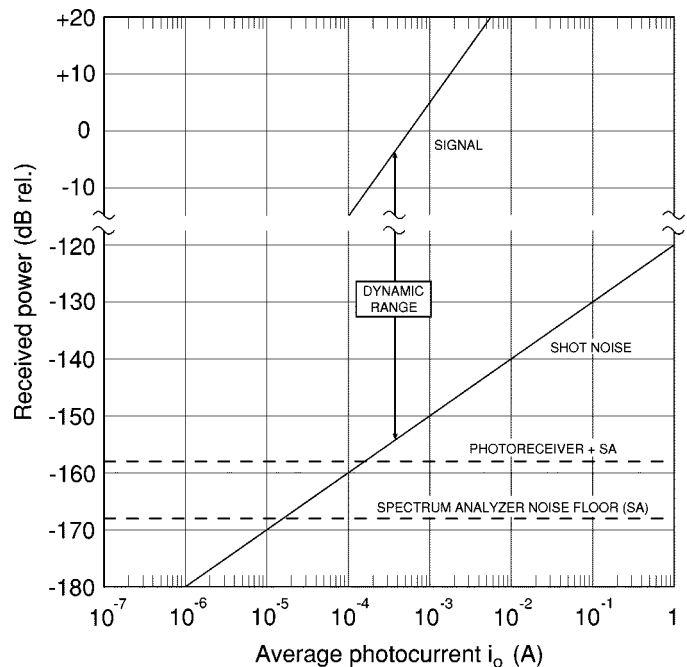


Fig. 3. Signal power and noise power spectral densities in the photoreceiver as a function of average photocurrent.

This is the maximum dynamic range achievable in the measurement of a conventional (nonsqueezed) laser light source since any amplitude modulation, no matter how small, cannot be detected below this shot-noise level.

To preserve the maximum dynamic range and the ultimate noise floor defined by the shot-noise limit, all electronic circuits following the photodetector must produce noise below the shot-noise floor. We are thus presented with the usual design philosophy of all receivers: let the noise contribution of all stages be less than that of the stages preceding them. In other words, let shot noise $>$ photoreceiver noise $>$ spectrum analyzer noise floor. Careful system engineering will preserve this situation. It is illuminating to simply plot the relevant signal contributions as a function of average photocurrent. Fig. 3 is a schematic representation of the trends in signal and noise powers. It shows that as the average photocurrent is increased, the shot noise eventually rises out of the electronic noise floor and the dynamic range improves at the rate of 10 dB/dec of photocurrent. This is the optimum region of operation since the minimum detectable modulation can now be measured. Further increases in the average photocurrent simply improve the dynamic range.

IV. SPECTRUM ANALYZERS

The main instrument responsible for frequency-domain analysis is the RF spectrum analyzer. It is used to measure the amplitude and phase-noise modulation spectra of the photoreceiver signal. The minimum detectable signal for this instrument is set by its own input noise floor and is usually specified in terms of an input equivalent noise voltage or power. In our system, we use an HP 3585A, which is specified to have a floor of -142 dBm/Hz (18 nV/ $\sqrt{\text{Hz}}$) but routinely displays a floor of about -147 dBm/Hz (10 nV/ $\sqrt{\text{Hz}}$). In either case, these noise floors are unacceptably high (requires $i_0 > 125$ mA), and it

is prudent to precede the analyzer with a good low-noise amplifier (LNA). This will lower the system noise figure to several decibels above kT and ensure shot-noise limited sensitivity. Our system has a 40-dB gain amplifier with a noise figure of better than 6 dB from 10 kHz to 40 MHz.

A typical RF spectrum analyzer has a useful frequency range of 100 Hz–1 GHz, and it is usually desirable to augment this with a lower frequency FFT analyzer with a range down to 0.01 Hz. The frequency boundary between the two instruments will be determined by the noise performance of each analyzer, its resolution bandwidth, and data acquisition speed. Modern spectrum analyzers frequently come equipped with a “noise measurement” function that calculates the noise power spectral density, taking into account the shape factors of the RF and IF filters in the analyzer. This feature should be exploited when measuring broadband noise, as it is not accurate to simply divide by the receiver’s -3 dB bandwidth. When encountering coherent signals (spurs), however, they must be left in terms of absolute power and not normalized to the receiver bandwidth (this issue is frequently overlooked).

V. PHOTORECEIVER DESIGN

A. Transimpedance Amplifiers

The measurement of shot noise on signals of large average photocurrent presents a somewhat different set of requirements from the usual optical signal detection. When we try to measure very low power signals with high modulation index, we usually use a transimpedance amplifier with very high feedback resistance to overcome the noise in following stages. For detecting high-speed optical data, we generally amplify the photodetector with broadband 50- Ω amplifiers. Neither of these approaches is necessarily optimum for our problem (high average current), and therefore it is useful to rethink the receiver design. The most obvious solution is to use a transimpedance configuration with a relatively low feedback resistance, which is required to keep the dc output voltage within the power-supply constraints. Owing to the prevalence of high-quality low-noise operational amplifiers, we use them in our baseband receiver circuits. Since the input resistance of the transimpedance configuration is extremely low, the circuit speed will be determined by photodiode and slew-rate limitations.

To optimize the photoreceiver design, we start by analyzing the noise contributions in a standard transimpedance amplifier and see how they vary as we adjust parameters such as feedback resistance, average photocurrent, and circuit component noise. The standard transimpedance amplifier shown as PR2 in Fig. 1 can be analyzed by taking account of all noise sources due to the photodiode, the feedback resistance, and the equivalent op-amp input voltage and current noise spectral densities [32], [33].

The equivalent circuit is shown in Fig. 4. The photodiode is modeled as having two current sources: one due to shot noise from the dark current and the other due to Johnson noise from the series combination of dynamic and series resistance. At the input of the op-amp are the input equivalent current and voltage noise sources, and around the feedback resistor is the current source due to Johnson noise. Since these noise sources are uncorrelated, we must add them on a mean-squared basis. There-

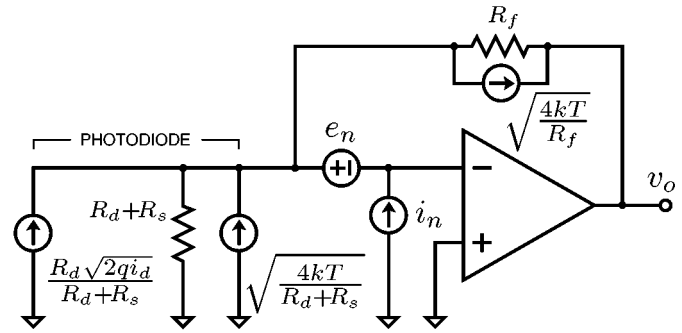


Fig. 4. Equivalent circuit of a transimpedance amplifier driven by a photodiode including noise sources.

fore the output mean-squared noise voltage spectral density becomes

$$\overline{v_o^2} = \left[\underbrace{\frac{2qi_d R_d^2}{(R_s + R_d)^2}}_{\text{DARK CURRENT SHOT NOISE}} + \underbrace{\frac{4kT}{R_s + R_d}}_{\text{PHOTODIODE JOHNSON NOISE}} + \underbrace{\overline{i_n^2}}_{\text{OP-AMP CURRENT NOISE}} + \underbrace{\frac{4kT}{R_f}}_{\text{FEEDBACK RESISTOR JOHNSON NOISE}} \right] R_f^2 + \underbrace{\overline{e_n^2}}_{\text{OP-AMP VOLTAGE NOISE}} \left(1 + \frac{R_f}{R_s + R_d} \right)^2 \quad \text{V}^2/\text{Hz} \quad (28)$$

where

- i_d dark current;
- i_n op-amp input noise current spectral density;
- e_n op-amp input noise voltage spectral density;
- R_d photodiode dynamic resistance;
- R_s photodiode series resistance.

Op-amp (or any electronic amplifier) noise performance is critical to achieving a low-noise photoreceiver. We used our RF and FFT spectrum analyzers to verify the equivalent input noise spectra of several op-amps [33] and chose the Burr-Brown OPA-643 based on a combination of factors including noise performance, speed, and availability.

Fig. 5 displays the variation in the mean-squared noise spectral density terms in (28) as a function of feedback resistance for the OPA-643. The sum of all noise sources is indicated by the dashed line. The dark current noise and photodiode Johnson noise are insignificant within the boundaries of this plot. The noise current (2.5 pA/ $\sqrt{\text{Hz}}$) and voltage spectral densities (2.3 nV/ $\sqrt{\text{Hz}}$) used were taken from the manufacturer’s data sheet. Notice that this receiver will be shot-noise limited for $R_f \gtrsim 150 \Omega$ with $i_0 = 1$ mA. Also, for $R_f > 10$ k Ω , we reach a point of diminishing returns since the shot-noise power/total-receiver-noise power becomes constant at about 15 dB.

Another important issue in transimpedance amplifiers running high average current is the maximum dc output voltage. To keep this within the power-supply limits, one must balance the needs of high average current and high feedback resistance. To see this interaction, Fig. 5 includes constant dc output voltage contours. For example, in order to maintain a 1-V dc output, operation on this contour would allow a feedback resistance of 1 k Ω at 1-mA average photocurrent. As a reasonable compro-

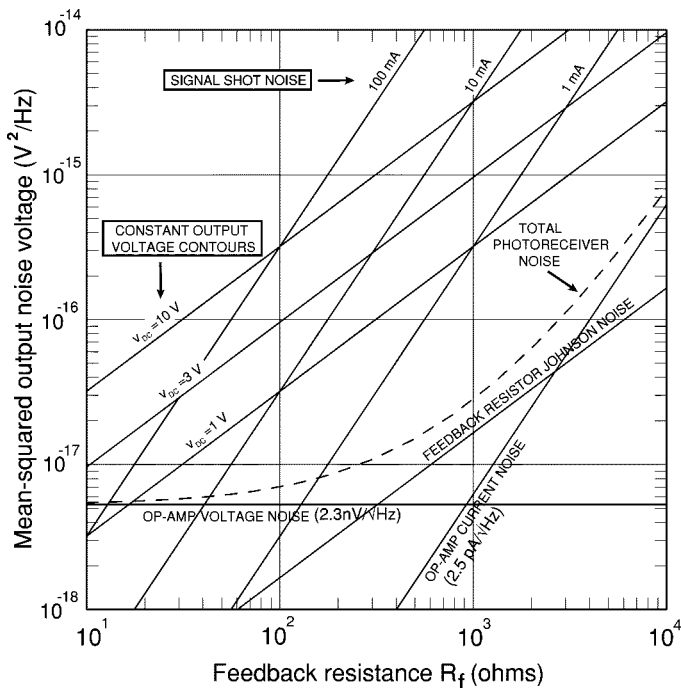


Fig. 5. Transimpedance photoreceiver mean-squared output noise voltage density as a function of feedback resistance R_f with constant dc output voltage contours. Mean-squared signal shot-noise voltage also shown for average photocurrents $i_0 = 1, 10, 100$ mA.

mise, we chose a feedback resistance of 330Ω and operate with $i_o \leq 6$ mA. To prevent saturation of the LNA following the photoreceiver, a dc blocking capacitor was used. For a $50\text{-}\Omega$ input resistance, this requires the capacitance $C > 2000 \mu\text{F}$ for a low-frequency RC cutoff of 1 Hz. This much capacitance can be a problem at high frequencies due to self-inductance. A buffer amplifier with a higher input impedance could be used to reduce C , but its noise characteristics would have to be reevaluated.

When making amplitude or phase-noise measurements of mode-locked lasers at the repetition frequency, one must consider output drive capabilities. The photoreceiver should be designed to drive $50\text{-}\Omega$ loads to be compatible with other system components (e.g., amplifiers, mixers, diode detectors, etc.). Mixers, when used as high-sensitivity phase detectors, require input powers in excess of $+15$ dBm ($3.6 V_{pp}$ in 50Ω). The slew-rate limit for most low-noise op-amps is well below what is required to run a 100-MHz signal at $+15$ dBm into 50Ω ($2200 V/\mu\text{s}$). We observed slew-rate limiting in the OPA-643 below these levels ($1000 V/\mu\text{s}$) and therefore chose to run the photodiode directly into the $50\text{-}\Omega$ input of a low-noise RF amplifier for phase-noise measurements. (Note: In general, these amplifiers do not extend to low enough frequency to use for baseband AM noise measurements and are not optimized for low-frequency noise performance.)

B. Photodiodes

In general, large-area photodiodes are required when driving high average currents, but this must be balanced against the need for measurement bandwidth. Also, at high currents, a photodiode begins to saturate and becomes nonlinear. This is even more serious for signals with a high peak-to-average ratio (i.e.,

pulses) since the photodiode will saturate at much lower average photocurrents [34]–[36]. This, in turn, seriously degrades the accuracy of noise measurements (Section VIII).

For each type of laser and measurement, we need to optimize the photodiode choice. Amplitude noise measurements of CW lasers require only moderate bandwidths (dc to tens of megahertz), and photodiodes that allow operation to $i_0 > 10$ mA at this bandwidth are readily available. Measuring the amplitude noise of mode-locked lasers at baseband has similar requirements, but the average current must be reduced because of saturation on the peaks. For amplitude and phase-noise measurements of mode-locked lasers at the repetition frequency, we need a photodiode that has a frequency cutoff $f_c > f_0 + \Delta f$, where Δf is the largest offset frequency of interest. This results in bandwidth requirements to hundreds of megahertz or more. Finding photodiodes that meet this requirement, and can run at high average current, can be difficult, and few manufacturers include saturation current in their data sheets. Recent work [37] in traveling-wave and waveguide p-i-n photodiodes has pushed the bandwidth limits of milliamp operation above 10 GHz.

C. Characteristics of the Photoreceivers

Amplitude noise measurements of the pump and Ti : sapphire lasers were made with a transimpedance amplifier using the Burr-Brown OPA-643 op-amp as discussed in Section V-A. The output has an impedance-matching $50\text{-}\Omega$ series resistor and a dc blocking capacitor of $2000 \mu\text{F}$. The photodiode was a Hamamatsu S3072 silicon p-i-n photodiode with a transit-time limited bandwidth of >45 MHz. It has an active area of 7 mm^2 , a terminal capacitance of 7 pF , a maximum bias voltage of 50 V , and a measured dc saturation current in excess of 10 mA . At that current, heating effects are the predominant limitation since the responsivity is only 0.35 A/W at pump laser wavelengths. In general, we were limited to a maximum current of 6 mA . To verify the noise characteristics of the op-amp, we measured the total output noise and compared it to the calculated output noise based on the manufacturer's data (Fig. 6).

The RC limited bandwidth of the transimpedance amplifier is 1 Hz – 220 MHz , with the lower frequency limit set by the capacitance of the dc block at the output of the photoreceiver and the upper limit set by the capacitance of the photodiode and the 800-MHz unity-gain bandwidth of the OPA-643. The gain and noise performance of the photoreceiver are shown in Fig. 7. Gain was measured by injecting a signal through a high resistance into the photodiode. The noise peak at 110 MHz is due to the standard noise gain of the transimpedance amplifier configuration [33] and is another reason why this configuration is difficult to use for carrier noise measurements.

Phase-noise measurements of a Ti : sapphire laser were made with a Hamamatsu S3883 silicon p-i-n photodiode followed by a 120-MHz low-pass filter (LPF) and an Avantek GPD-405 RF amplifier. The photodiode has a transit-time-limited bandwidth of 300 MHz , an active area of 1.7 mm^2 , a terminal capacitance of 6 pF , and a maximum bias voltage of 30 V . We measured the dc saturation current to be $>6 \text{ mA}$. However, due to the high peak-to-average current ratio, we were limited to a maximum average current of 2.5 mA . The GPD-405 amplifier has 13 dB of gain from 10 to 400 MHz and a noise figure of

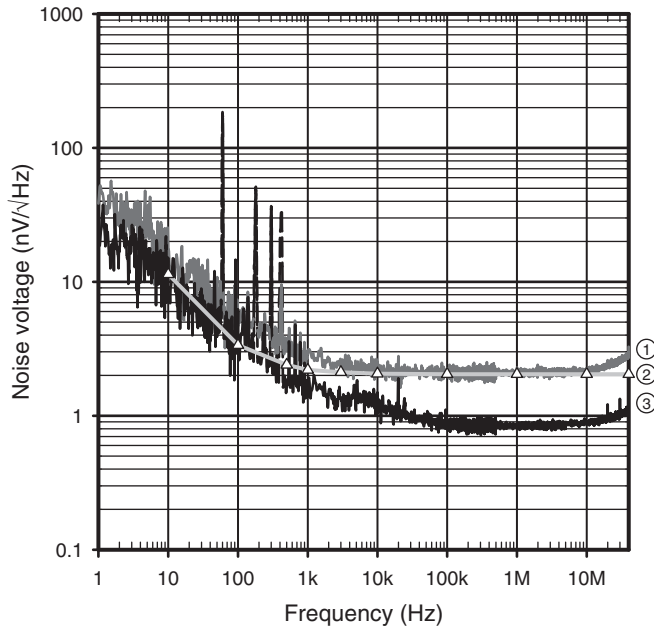


Fig. 6. Measured and calculated electronic noise at the output of the photoreceiver used for amplitude noise measurements. ① Measured amplitude noise of photoreceiver. ② Calculated noise at output of photoreceiver based on manufacturer's data (Δ). ③ Measurement system noise floor.

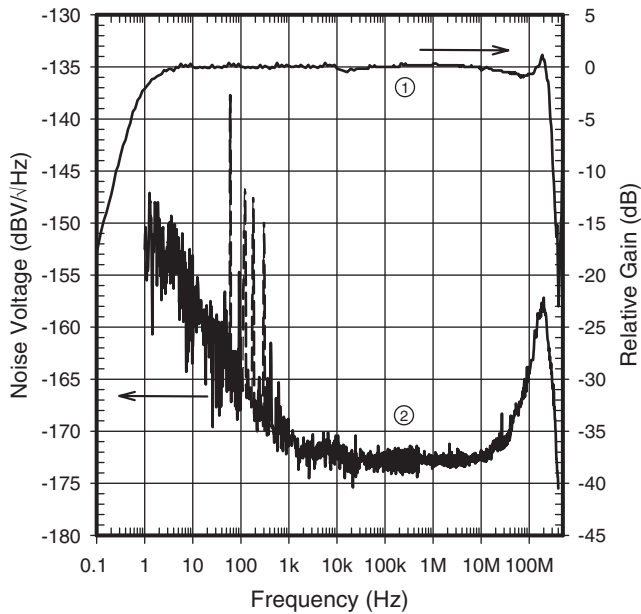


Fig. 7. Photoreceiver gain and noise. ① Relative gain in dB with respect to a nominal gain of 330 V/A. ② Noise voltage at photoreceiver output.

<5 dB. The 120-MHz filter is necessary to reduce the second and higher order harmonics from the photoreceiver since the amplifier cannot tolerate the high peak voltages of the pulses.

VI. THE COMPLETE SYSTEM

The essential components for making amplitude and phase-noise measurements are shown in Fig. 1. With the exception of the photoreceiver, these are the same components required to make amplitude and phase-noise measurements of RF and mi-

crowave sources. Many years of research and development have gone into optimizing these components and creating integrated measurement systems, including software control. We take advantage of this by using one of the first complete systems developed for phase-noise measurement; the HP 3047A. (These systems are not the same as the "phase-noise measurement utility" available on some spectrum analyzers.) However, it is not necessary to have a commercial system in order to make reliable, high-dynamic-range noise measurements. One can assemble the essential components and, using modern software tools, create an equivalent system. The commercial systems eliminate the arduous tasks associated with measurement calibration, normalization, data acquisition and display, instrument control, and stitching together data from the various frequency bands. The reader is cautioned, however, to realize that replicating and verifying a reliable AM/PM noise measurement system is a formidable project. The software that controls the HP 3047A has in excess of 10 000 lines of BASIC code.

The HP 3047A consists of two spectrum analyzers: a spectrum analyzer interface and a computer running the measurement software. The low-frequency FFT analyzer, an HP 3582A, has a frequency range from 0.01 Hz to 25 kHz and a noise floor of -140 dBm/Hz (>1 kHz). The RF spectrum analyzer, an HP 3585A, covers the range from 20 Hz to 40 MHz and has a noise floor of -147 dBm/Hz (>20 kHz). Together, these spectrum analyzers allow us to make noise measurements at offset frequencies from 0.02 Hz to 40 MHz. In this range, we readily observe noise with mechanical origins such as optical mount and electrical cable vibrations, instrument fan vibrations, general laboratory acoustical noise coupled into the laser signal, and low-frequency electrical interference such as power line or switching supply spurs (1 Hz–500 kHz). We can also see higher frequency electrical interference, thermal noise, laser relaxation oscillations, shot noise, and more.

Since the spectrum analyzers have noise floors approximately 30 dB above thermal noise ($kT = -174$ dBm/Hz), a low-noise amplifier is included in the spectrum analyzer interface box (HP 35601A). With 40 dB of gain and a noise figure (NF) of 5 dB ($f \gtrsim 10$ kHz), the absolute system noise floor is reduced to -169 dBm/Hz and all measured noise, e.g., laser shot noise, must be greater than this value.

The interface box also includes a 5 MHz–1.6 GHz mixer used as a phase detector. A 60-MHz LPF is used to remove the second- and higher order harmonics that are present at the output of the phase detector. It is important to use a multipole, constant-impedance LPF so that the large second harmonic signal is not reflected back into the mixer, degrading detector performance, or passed through to the LNA. In addition, there is a remotely programmable phase-locked loop (PLL) for frequency control of voltage-controlled oscillators (VCOs). This allows the system to keep two sources (e.g., mode-locked laser and reference oscillator) in quadrature during a measurement.

All of the components of the measurement system must be connected with high-quality cables and connectors. Double-shielded or semi-rigid coax should be used whenever possible. The instruments and cabling should be securely mounted to minimize microphonic effects, and every effort should be made to minimize ground loops [38].

VII. SYSTEM CALIBRATION

One of the most important, and frequently overlooked, elements in making reliable noise measurements is system calibration. It is one of the most difficult and time-consuming aspects of the measurement process. At a minimum, the following must be characterized over the entire frequency range of interest (dc–40 MHz for AM noise and 40–120 MHz for PM noise), photoreceiver and amplifier gain and noise, filter bandwidths, and spectrum analyzer response (noise floor). In addition, for phase-noise measurements, we need to know the phase detector constant, PLL response when using a VCO, absolute phase noise of any reference oscillators, and residual phase noise of all amplifiers used.

A. System Amplitude Noise Floor

Once a noise measurement system has been assembled, the noise floor must be continually verified. In our experience, when the setup location or environmental conditions change, a noise floor may no longer be valid. Since we are looking at such small signal levels (<1 nV/ $\sqrt{\text{Hz}}$), even cable placement can make a 20-dB difference in a spur level. Ground loops are especially troublesome. Good electrical engineering practices must be used [38] during the design and construction of the system. All components and their power supplies must be considered.

For amplitude noise measurements, the absolute voltages measured by the spectrum analyzers are compared with the dc voltage at the photoreceiver output, which is proportional to the average photocurrent. The ratio then establishes the relative intensity noise (RIN) as a spectral density (dB/Hz). To observe the full dynamic range available, it is essential that the system noise floor be below that of the photoreceiver, which in turn must be below the shot noise. System noise floor verification is accomplished by terminating the input of the LNA in its characteristic impedance (50Ω) and making a full measurement. System and environmental noise sources can then be recognized and minimized. External noise sources that we have generally observed include cable vibration, ac power line spurs, switching power-supply spurs, magnetic fields from transformers of nearby instruments, fans, system ground loops, computers and other digital equipment in the vicinity, CRTs, and high-power RF sources (Pockels cell drivers, induction heaters, etc.). A significant improvement in power line spur interference can be realized by powering the LNA and associated control circuitry within the HP 35601 with batteries [Fig. 8(a)]. We used sealed lead–acid types that are only switched in when an actual measurement takes place.

The photoreceiver noise floor can be verified after the system noise floor has been established. We also used batteries to power the photoreceiver and obtained a substantial improvement in noise floor performance [Fig. 8(b)]. In subsequent data plots, we show the total system noise floor obtained during a measurement, which is an important aspect of data presentation.

B. Measuring the Phase Detector Constant K_ϕ

Accurate phase-noise measurements require careful measurement of the phase detector constant K_ϕ . This is the critical link between phase modulation and the measured signal out of the

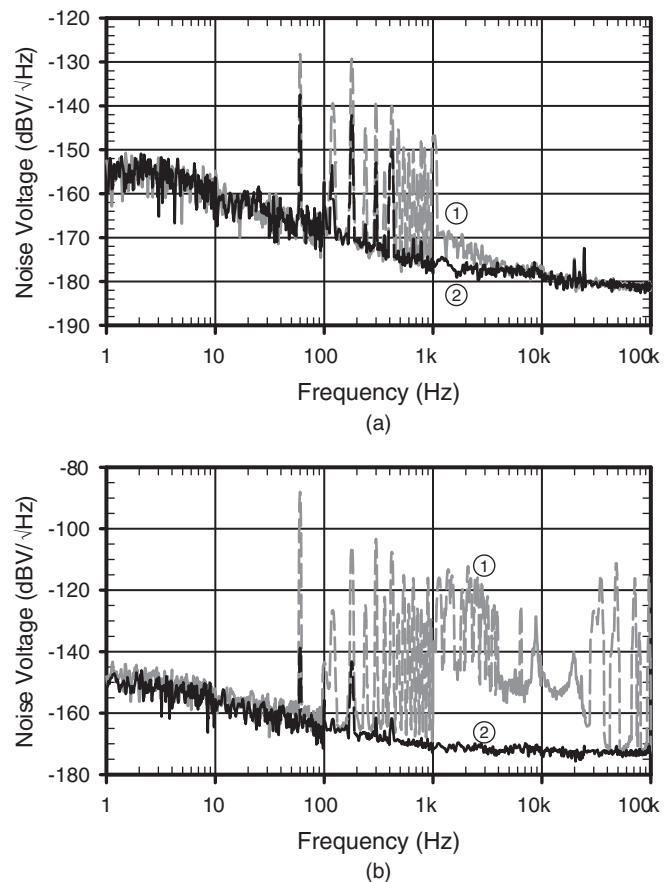


Fig. 8. Noise floor of measurement system and photoreceiver showing the improvement realized when the HP 35601 and photoreceiver are powered from batteries. (a) Input noise of HP 35601 (LNA + spectrum analyzers). ① Powered from the AC line. ② Powered from battery source. (b) Output noise of photoreceiver PR2. ① Powered from a bench power supply (HP 6205B). ② Powered from battery source.

phase detector (23). There are four common methods for establishing K_ϕ .

1) *FM/PM Double-Sideband Modulation Method*: In the FM/PM modulation method, one of the two signals entering the phase detector has a low-level FM or PM modulation applied to it at frequency ω_m . Ideally, this would be the reference oscillator at the LO port since the accuracy of the calibration technique relies on signals at the mixer's being identical to those under actual measurement conditions. With the two ports in phase quadrature ($\theta = \pi/2$), the LO port is driven with the PM signal $v_{\text{LO}}(t) = V_{\text{LO}} \cos(\omega_0 t + \beta \sin \omega_m t)$, which has an rms phase deviation $\beta/\sqrt{2} \ll 1$. The voltage at the IF port of the mixer will be, from (19)

$$v_{\text{IF}}(t) = \frac{\alpha}{2} V_{\text{LO}} V_0 \beta \sin \omega_m t \quad (29)$$

and the phase detector constant is, from (22)

$$K_{\phi} \left[\frac{\text{DSB}}{\text{PM}} \right] \equiv \frac{\sqrt{v_{\text{IF}}^2}}{\sqrt{\phi^2}} = \frac{\sqrt{v_{\text{IF}}^2}}{\beta/\sqrt{2}} = \sqrt{\frac{v_{\text{IF}}^2}{2}} \frac{P_c}{P_{\text{sp}}} \text{ V/rad} \quad (30)$$

where we have used (6) to relate β to the single-sideband PM spur-to-carrier ratio P_{sp}/P_c in the small angle approximation.

In practice, we use a separate spectrum analyzer to measure the ratio P_{sp}/P_c . Combining this with the measured rms IF voltage in (30) yields the phase detector constant K_ϕ .

Now all spectra measured by the system can be converted to SSB phase-noise spectral density referred to one side of the carrier. The spectrum analyzers measure a noise voltage spectral density $V_{IF}(f)$ (V/ $\sqrt{\text{Hz}}$). Dividing by K_ϕ and squaring gives

$$S_\phi(f) = \left[\frac{V_{IF}(f) (V/\sqrt{\text{Hz}})}{K_\phi (V/\text{rad})} \right]^2 \text{ rad}^2/\text{Hz} \quad (31)$$

and, finally, $\mathcal{L}(f) = S_\phi(f)/2$.

2) *Single-Sided Spur Method*: In the single-sided spur method, we inject a low-amplitude sinusoid adjacent to the carrier, on either side, with power level P_{sp} . From Section II-C, we know that this single-sided spur can be decomposed into two PM and two AM sidebands. The phase detector is not sensitive to the AM terms but produces an output voltage due to the carrier being modulated by the two PM sidebands with single sideband spur-to-carrier ratio $P_{sp}/4P_c$. If we independently measure the ratio P_{sp}/P_c on another spectrum analyzer, we can use our previous result (30) provided we correct the ratio by a factor of four. Thus

$$K_\phi \left[\begin{smallmatrix} \text{SSB} \\ \text{SPUR} \end{smallmatrix} \right] \equiv \frac{\sqrt{v_{IF}^2}}{\sqrt{\phi^2}} = \sqrt{2v_{IF}^2 \frac{P_c}{P_{sp}}} \text{ V/rad}. \quad (32)$$

Both the double-sideband FM/PM and the single-sided spur technique have very high accuracy since they are done under actual measurement conditions using all of the system components in place for a phase-noise measurement. All component gains, losses, and nonlinearities are absorbed into K_ϕ and later divided out of the data. For the FM/PM technique, the reference signal generator is phase modulated with sidebands at -30 to -60 dBc; or, in the case of high-stability crystal oscillators, an external phase modulator can be used. For the single-sided spur technique (our preferred method), a power combiner or directional coupler can be used to inject a low-level spur without affecting the impedance of the lines between the generator and the mixer.

3) *Static Phase Slope Method*: This method requires a line stretcher or phase shifter that allows the phase of one of the mixer signals to be adjusted over a range about quadrature. The dc output of the phase detector is observed on an oscilloscope while the phase is adjusted symmetrically about quadrature by a very small amount $\pm\delta\phi$. The ratio of the measured voltage deviation $\pm\delta V$ to the static phase shift gives the static phase slope: $K_\phi = \delta V/\delta\phi$. This method is less accurate than the previous two since one must independently measure the ac gain from the mixer to the spectrum analyzers and apply it to evaluating the ac value of K_ϕ . Also, small nonlinearities or asymmetries in the mixer response do not manifest themselves in this static test.

4) *Beat Note Method*: In the beat note method, both signals are connected to the input ports of the mixer, but one is tuned off the carrier to produce a beat note at the difference frequency. Suppose the reference oscillator driving the LO port is detuned

by an amount ω_1 from the carrier. After low-pass filtering, the output of the mixer is

$$v_{IF}(t) = \frac{\alpha}{2} V_{LO} V_0 \sin \omega_1 t. \quad (33)$$

The amplitude of this mixing product gives us direct knowledge of the product $\alpha V_{LO} V_0$. We can use this with the development of K_ϕ for the FM/PM spur case above by combining (29) and (30) in a slightly different way

$$K_{\phi[\text{BEAT}]} \equiv \frac{\sqrt{v_{IF}^2}}{\sqrt{\phi^2}} = \frac{\frac{\alpha}{2\sqrt{2}} V_{LO} V_0 \beta}{\beta/\sqrt{2}} = \frac{\alpha}{2} V_{LO} V_0 \text{ V/rad}. \quad (34)$$

Thus, the peak value of the beat note is equal to the phase detector constant. This expression is general and pertains to both the FM/PM case and the beat-note case. We could, in fact, use this for the FM/PM method, but it would require separate measurements of the IF voltage and the modulation index, which would be divided out of (29). The beat-note method (34) simply requires measurement of a peak voltage, which is available from the spectrum analyzers and includes all of the gain and loss of the intervening circuits. It is an excellent method and comparable in accuracy to FM/PM and the single-sided spur method.

C. System Phase-Noise Floor

In a phase-noise setup, system noise floor verification is accomplished by driving both ports of the phase detector with a common low-noise RF source through a power splitter. The source's phase noise at the input of the phase detector is correlated and does not appear at the output. An adjustable RF delay line can be used at one port to obtain quadrature; however, the total delay between the power splitter and phase detector must be kept to a minimum so that the noise does not decorrelate at higher offset frequencies. A typical phase-noise floor is shown in Fig. 9 for $+12$ and $+15$ dBm at 80 MHz at the RF and LO ports, respectively. Running the interface box on batteries also shows a definite improvement in the phase-noise floor.

D. Data Interpretation and Presentation

Noise measured in the frequency domain is primarily a spectral density. The spectrum analyzers measure the absolute power within their filter bandwidths, and it is common to normalize these data to a power or voltage spectral density. One must be careful not to use the resolution bandwidth of the spectrum analyzer directly when normalizing the noise data to a 1-Hz bandwidth. Instead, the noise-equivalent filter bandwidth, which includes the filter shape, should be used. Additionally, if the spectrum analyzer has a noise measurement function, this can be used directly, or its result can be used to deduce the equivalent filter bandwidth. When taking data, frequency spans and filter bandwidths must be chosen to optimize resolution and scanning speed, and some averaging should be applied to improve the estimate of the mean-squared quantities. Also, data should be taken and plotted in equal logarithmic intervals, if possible.

When plotting the data, it is useful to mark coherent signals within the noise plot since these signals should not be normal-

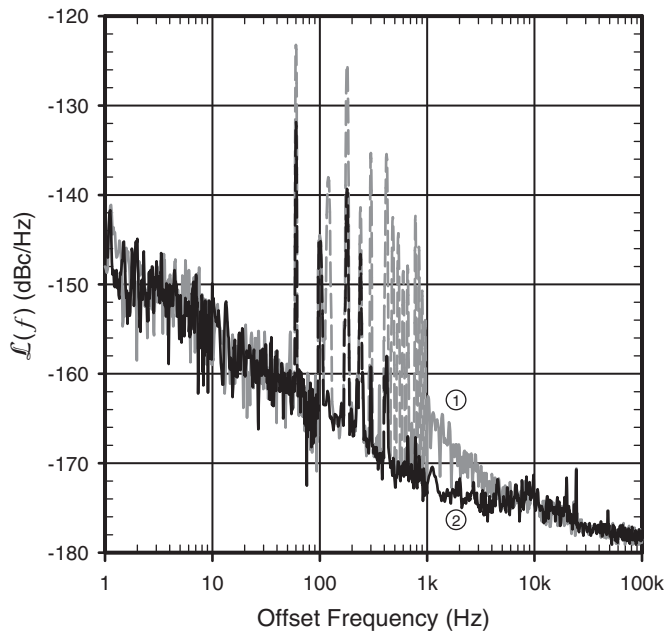


Fig. 9. SSB phase-noise floor of our measurement system at low offset frequencies showing the improvement realized when the HP 35601 is powered from batteries. Phase detector input frequency is 80 MHz. ① Powered from the ac line. ② Powered from battery source.

ized to a 1-Hz bandwidth and instead presented at their true level. A common convention is to show coherent signals as dashed or dotted lines, while the noise data is shown as a solid line. The software that controls the HP 3047A and similar systems has algorithms for deciding whether a pathological data point is a coherent spur. These algorithms depend on the values of adjacent data points, the number of averages, etc. [30]. Single data point spurs are not marked. This is by no means a fool-proof method of picking out spurs, and sometimes it marks small breaks in the noise as a spur. However, it simplifies interpretation of the data.

Amplitude and phase-noise data should be plotted in relative terms (e.g., dBc/Hz, RIN, % rms, etc.). Doing so allows measurements taken under different operating conditions, and on different devices, to be compared without transformation. In the optics community, it is common to plot amplitude fluctuations in terms of RIN, where RIN is defined as the ratio of the mean-squared optical noise power (\mathcal{P}_n) to the square of the average optical power (\mathcal{P}_0)

$$\text{RIN} = \frac{\langle \mathcal{P}_n^2 \rangle}{\mathcal{P}_0^2} \quad \text{and} \quad \text{RIN}[\text{dB}] = 10 \log(\text{RIN}) \quad (35)$$

where $\mathcal{P}_n^2 \propto P_n$ (electrical noise power) and $\mathcal{P}_0^2 \propto P_c$ (electrical carrier power). Thus, RIN is equivalent to plotting amplitude noise in dBc and may also be redefined to represent a spectral density $\text{RIN}(f)$ with units of dB/Hz. Many laser manufacturers present amplitude noise in %rms, which is the $\text{RIN}(f)$ integrated over a stated bandwidth. However, as laser sources become more stable, this representation gets cumbersome (e.g., 0.0001% rms noise from 10 Hz to 10 MHz). It is much more valuable to present the amplitude noise spectral density.

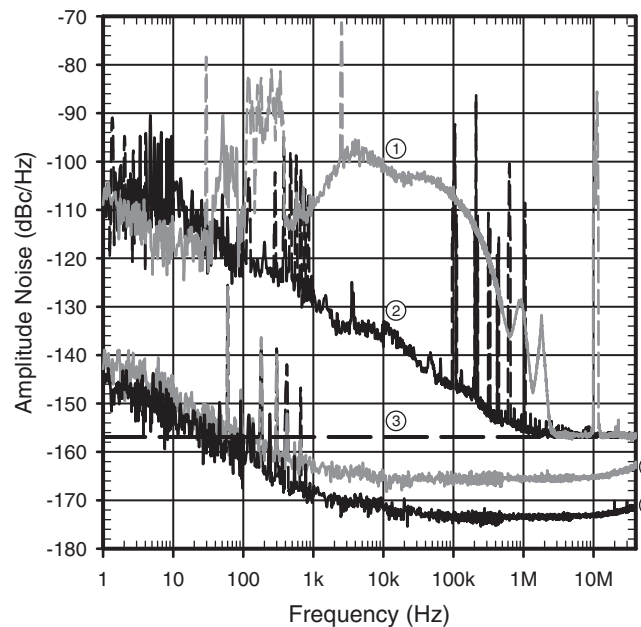


Fig. 10. Amplitude noise of argon-ion and DPSS lasers, $i_0 = 2.5$ mA. ① Argon-ion laser noise. ② DPSS laser noise. ③ Calculated shot-noise limit. ④ Photoreceiver noise floor. ⑤ System noise floor.

VIII. AM NOISE MEASUREMENTS

A. Measurement of Amplitude Noise in CW Lasers

Using the transimpedance amplifier of Section V-C, we have measured the amplitude noise of two different pump lasers and a Ti:sapphire laser operating with each pump. The first pump laser we investigated was a Coherent I-310 argon-ion laser running multiline visible with an output power of 5 W. The light regulation mode was enabled, reducing the amplitude noise for frequencies less than 2 kHz. Warmup times were always in excess of 1 h to guarantee stable operation. The other pump laser was a Coherent Verdi-V5 DPSS laser running at 5 W.

The measurements were shot-noise limited at -157 dBc for an average photocurrent of 2.5 mA. The AM noise measurement for either laser delivers extremely close agreement with the calculated shot-noise floor (Fig. 10). This agreement was achieved for arbitrary photocurrents above the photoreceiver noise floor, up to photodiode saturation. Notice that the lasers have similar low-frequency performance (< 50 Hz); however, from 100 Hz to 1 MHz, there is up to a 30-dB difference in the amplitude noise. The DPSS laser shows large spurs at 100 kHz and its harmonics originating from the switching power supply. The amplitude noise plots can be integrated from 1 Hz to 40 MHz and cast in terms of total rms noise. The argon-ion laser noise is 0.21% rms and the DPSS laser noise is 0.011% rms.

When the photodiode began to saturate, it first appeared as a rolloff of the high-frequency amplitude noise. If the saturation was severe enough, it caused the apparent noise floor to drop below the shot-noise limit [Fig. 11 ②]. This was a localized saturation effect, caused by tight focusing of the beam onto part of the photodiode's active area by means of a short focal length lens. The high flux density at the focus caused a localized saturation and therefore inhibited linear operation of the

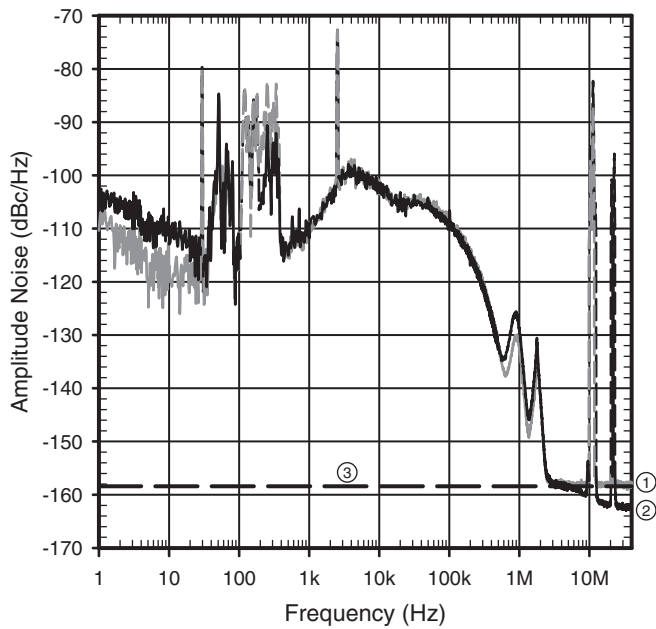


Fig. 11. Amplitude noise of argon-ion laser showing effect of photodiode saturation, $i_0 = 2.5$ mA. ① No saturation. ② Saturation caused by tight focusing. ③ Calculated shot-noise limit.

device. This problem can be circumvented by defocusing the beam or by using an iris, instead of a lens, to restrict the beam to the active area of the detector. Overfilling the iris creates a more uniform flux density at the same average current. However, beam steering becomes more of a problem in this setup, and the sensitivity to mechanical vibrations increases. This mandates that the measurement be made very near (< 1 m) the laser output with a minimum of optical components (beam pickoffs, turning mirrors, attenuators, etc.). A further increase in saturation current was realized by biasing the photodiode very near the maximum rating ($V_{\text{bias}} > 0.95 \cdot V_{R_{\text{max}}}$). We saw significant improvement in the saturation current even with small changes in the bias voltage.

B. Amplitude Noise of a Mode-Locked Ti:sapphire Laser

The amplitude noise of a mode-locked laser can be measured at baseband, at the repetition frequency, or at a harmonic. A diode detector is generally used to measure amplitude noise at the carrier or harmonic; however, there are some serious disadvantages to using a diode detector. Calibration is somewhat complicated: there is conversion loss, carrier feedthrough must be minimized, and a diode detector has a high-pass filter characteristic. This can restrict offset frequencies at lower repetition rates. Furthermore, there is a threshold effect that invalidates low-amplitude signals [29]. These problems are avoided by making the measurement at baseband. Additionally, the requirements on photoreceiver bandwidth are limited to the largest offset frequency of interest. Calibration is straightforward: since there is a dc signal (carrier), the noise is an absolute power and the ratio is all that is required for $\text{RIN}(f)$.

We used a KMLabs model TS Ti:sapphire laser for all of our mode-locked laser measurements. The laser was assembled on a Super Invar breadboard and generated an average output

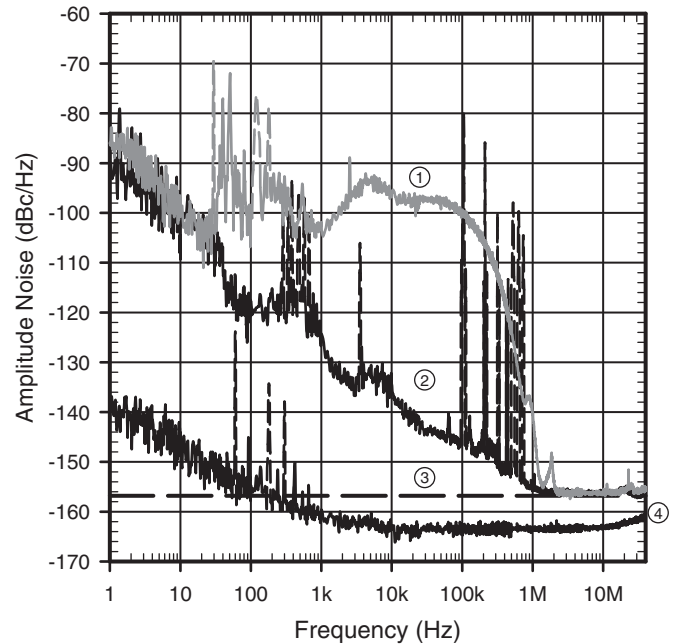


Fig. 12. Amplitude noise of Ti:sapphire laser with two different types of pump laser, $i_0 = 2$ mA. ① Argon-ion pump. ② DPSS pump. ③ Calculated shot-noise limit, including photoreceiver noise. ④ Photoreceiver noise floor.

power of 750 mW with 5 W of pump power. To facilitate other experiments, it was necessary to locate the pump lasers ~ 2.5 m from the Ti:sapphire laser. To minimize the detrimental effects, we used high-quality mounts for our turning mirrors and enclosed the full length of the pump beam in hard tubing. The mode-locked operation was very stable and allowed continuous operation in excess of 8 h. To allow sensitive phase-noise measurements, we phase-locked the laser to an 80-MHz crystal standard by incorporating a PZT Pusher (Burleigh PZ-30) behind the high-reflector mirror in the laser cavity (Section IX) [39].

The amplitude noise of the Ti:sapphire laser was measured at baseband with our transimpedance amplifier (Section V-C). To avoid saturation of the LNA, a dc block and 50-MHz LPF were placed after the photoreceiver. A typical noise plot is shown in Fig. 12 at an average photodetector current of 2 mA, shot-noise limited at -157 dBc/Hz. The correlation with the AM noise of the pump lasers (Fig. 10) is striking, and attenuation of pump noise above 300 kHz due to the $3.2\text{-}\mu\text{s}$ fluorescent lifetime is also evident. The integrated amplitude noise was 0.50% rms with the argon-ion pump and 0.015% rms with the DPSS pump (both integrated over 1 Hz–40 MHz). Note that noise data were taken with the PLL circuit both active and powered down, and no difference in the results was observed.

IX. PHASE-NOISE MEASUREMENTS

Laser phase-noise measurements were made at the fundamental frequency (80 MHz) using PR1 described in Section V-C. Measurements of absolute phase noise require a reference oscillator that is at least 10 dB lower in phase noise than the source under test over all offset frequencies. Phase-noise measurements place a slightly greater requirement on system noise performance than amplitude noise measurements.

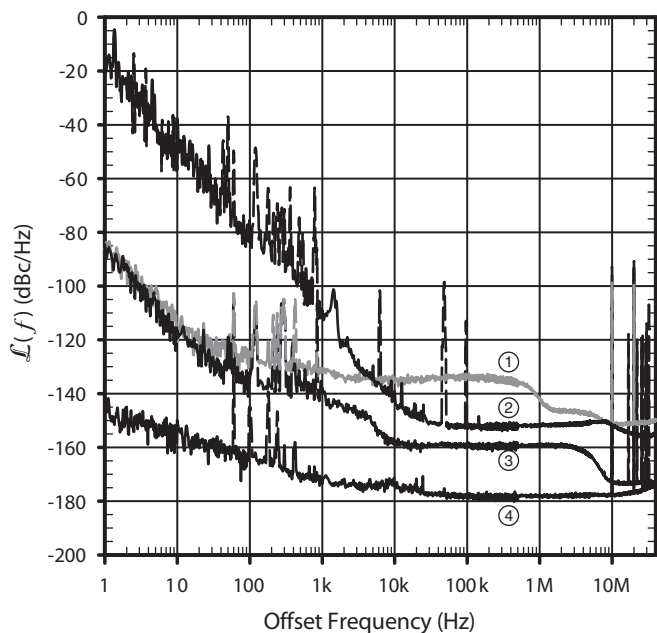


Fig. 13. Absolute SSB phase noise of various RF sources operating at 80 MHz. ① HP 8662A synthesized output. ② HP 8640B using DCFM. ③ HP 8662A's internal 10-MHz crystal oscillator and $8\times$ multiplier chain versus similar 10-MHz crystal oscillator with $8\times$ multiplier chain. ④ Worst case system phase noise floor, +12 dBm at RF port and +15 dBm at LO port.

Equation (27) gives the shot-noise floor compared with the average photocurrent. When making phase-noise measurements, we are dealing with the phase-noise component of the shot noise adjacent to the carrier. Shot noise, with a white spectral density, is evenly split between phase and amplitude modulation of the carrier and lowers the phase-noise floor by 3 dB. Also, a Fourier series expansion of the photocurrent

$$i(t) = \frac{a_0}{2} + \sum_{n=1}^{\infty} a_n \cos(n\omega_0 t) + b_n \sin(n\omega_0 t) \quad (36)$$

where

$$a_n = \frac{2}{T} \int_{-T/2}^{+T/2} i(t) \cos(n\omega_0 t) dt \quad (37)$$

$$b_n = \frac{2}{T} \int_{-T/2}^{+T/2} i(t) \sin(n\omega_0 t) dt \quad (38)$$

and $\omega_0 = 2\pi/T$ shows that, for a short pulse, any of the harmonic components have twice the power of the average or dc term. This accounts for another 3 dB. Thus, adjacent to the fundamental, or any harmonic of the laser pulse repetition rate, the single-sideband shot-noise-to-carrier power ratio in a phase-noise system is given by -161 dBc/Hz at $i_0 = 1$ mA and decreases by 3 dB for each doubling of i_0 . This means that in order to be shot-noise limited, the reference oscillators with which we compare the lasers must have phase-noise floors substantially below this. This is a rather tall order for synthesizers by today's standards, and the only oscillators that currently meet this requirement are fixed quartz crystal standards followed by low-phase-noise multipliers. This is what we use.

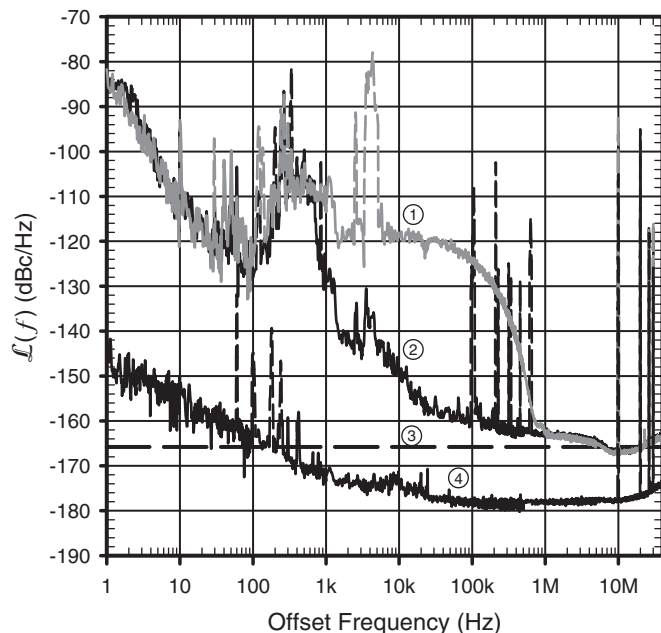


Fig. 14. Absolute SSB phase noise of phase-locked Ti:sapphire laser at 80 MHz with two different types of pump laser, $i_0 = 3$ mA. ① Argon-ion pump. ② DPSS pump. ③ Calculated shot-noise limit. ④ Worst case system phase-noise floor, +12 dBm at RF port and +15 dBm at LO port.

To demonstrate our point, consider Fig. 13, which shows the phase noise at 80 MHz of two high-quality commercial signal generators compared with a 10-MHz crystal oscillator multiplied up to 80 MHz. Low-phase-noise RF synthesizers and generators are inadequate reference oscillators for laser phase-noise measurements. The low-frequency phase noise of these sources operating in direct-coupled frequency modulation (DCFM) mode is especially poor. Our reference source uses an HP 10811B 10-MHz oven-controlled crystal oscillator and an $8\times$ multiplier chain, with ± 4 Hz of electronic tuning. We followed the multiplier chain with an 80-MHz bandpass filter (± 4 MHz BW) to strip off the noise sidebands, as shown by Fig. 13, trace ③. This allows us to see the laser shot-noise floor in the 7–40 MHz regime. The system noise floor, Fig. 13, is trace ④, -178 dBc/Hz at the port powers indicated. It improves to -181 dBc/Hz for $\geq +15$ dBm at each phase detector port.

During a measurement, source quadrature is maintained by the adjustable PLL within the HP 35601A. Normally, this would invalidate phase noise data within the loop bandwidth. However, the system carefully measures the PLL transfer function and backs out its effect [30].

Without a separate PLL controlling the Ti:sapphire frequency, we saw a drift rate of ~ 0.5 Hz/min. This frequency drift, and short-term frequency jitter, would require us to have >1 kHz of DCFM bandwidth to maintain quadrature during a phase-noise measurement, which requires 15–20 min. However, RF sources with large DCFM bandwidth do not have sufficiently low phase noise to observe the laser's phase noise. Therefore, we always phase-locked the laser repetition frequency to a 10-MHz crystal + $8\times$ multiplier chain. The laser's PLL is a standard wide-bandwidth design [40] with a "natural" frequency $f_n = 700$ Hz, limited by the first PZT resonance at 1.2 kHz.

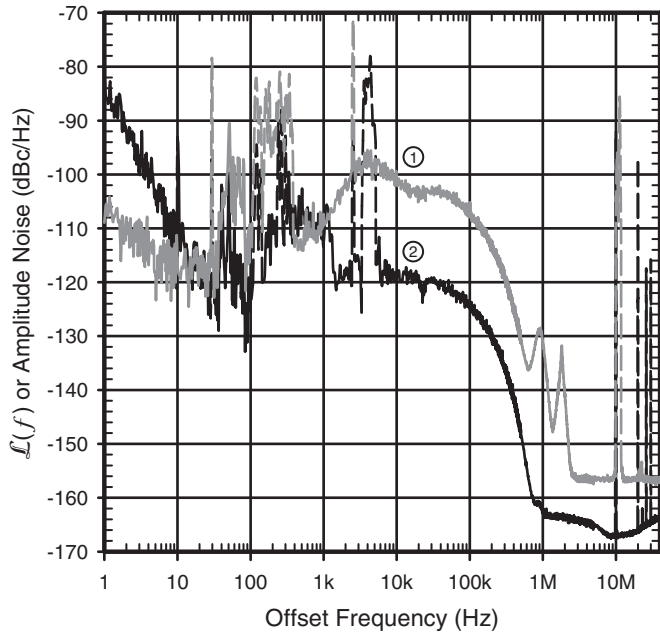


Fig. 15. Overlay of Ti:sapphire SSB phase noise, $\mathcal{L}(f)$, and the amplitude noise of its argon-ion pump laser. ① Argon-ion laser amplitude noise at baseband, $i_0 = 2.5$ mA. ② Ti:sapphire laser SSB phase noise at 80 MHz, $i_0 = 3$ mA.

Absolute phase-noise data for the phase-locked Ti:sapphire laser versus an 80-MHz multiplier chain are shown for two different pump lasers in Fig. 14. The shot-noise-limited phase noise floor is -165.8 dBc/Hz at $i_0 = 3$ mA. Within the laser's PLL bandwidth, the phase noise is limited to that of the laser's reference. As the gain of the laser's PLL rolls off ($f > 100$ Hz), the environmental disturbances (mount vibrations, air currents, etc.) increase the phase noise. The measured phase noise in the 300 kHz–7 MHz region is limited by the phase noise of the 80-MHz multiplier chain reference oscillator. Beyond 7 MHz, the phase noise is shot-noise limited.

If we integrate the phase-noise spectra shown in Fig. 14, we can calculate an approximate rms timing jitter, assuming minimal influence from pulsewidth and pulse-energy fluctuations [25]–[28], according to

$$\Delta t_{\text{rms}} = \frac{1}{n\omega_0} \sqrt{2 \int_{f_1}^{f_2} \mathcal{L}(f) df} \quad (39)$$

where n is the measured harmonic and f_1 and f_2 are the low and high offset frequencies adjacent to the carrier. With the argon-ion pump laser, $\Delta t_{\text{rms}} = 1.04$ ps, and with the DPSS pump laser, $\Delta t_{\text{rms}} = 0.74$ ps (1 Hz–40 MHz).

AM-to-PM conversion is a significant issue when trying to reduce the timing jitter of an optically pumped mode-locked laser. Figs. 15 and 16 show an overlay of the pump laser amplitude noise with the Ti:sapphire phase noise. Note the striking correlation between the amplitude and phase-noise spectra in each plot. We believe that this is due to gain variation with pump variation and thus a change in index of refraction and cavity length.

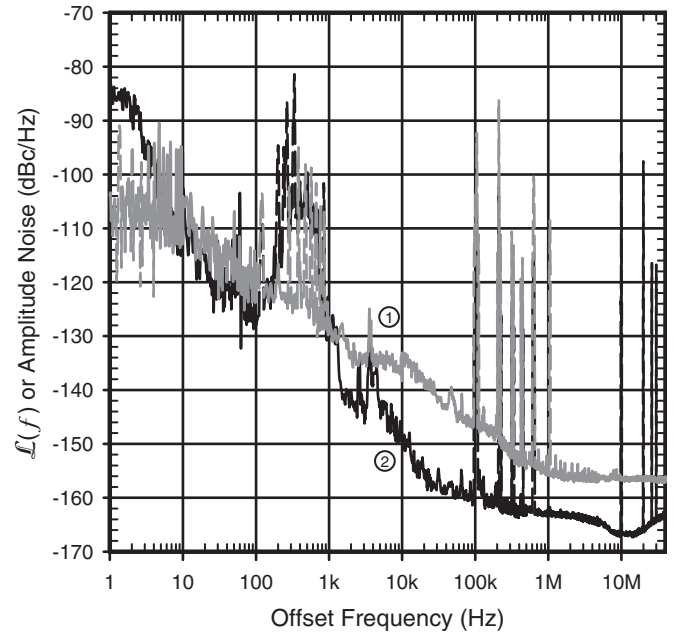


Fig. 16. Overlay of Ti:sapphire SSB phase noise, $\mathcal{L}(f)$, and the amplitude noise of its DPSS pump laser. ① DPSS laser amplitude noise at baseband, $i_0 = 2.5$ mA. ② Ti:sapphire laser SSB phase noise at 80 MHz, $i_0 = 3$ mA.

X. CONCLUSION

Characterizing the amplitude and phase noise (timing jitter) of modern lasers is becoming a challenging task owing to their current and ever-improving levels of performance. In this paper, we have set forth the fundamental issues associated with these demanding measurements. Critical to all phases of the work is understanding and minimizing extraneous noise due to system components as well as environmental effects. Also, a clear understanding of the dynamic range requirements as defined by shot noise is necessary. We have shown that for baseband measurements of amplitude noise (the preferred method), the system noise floor must be $\ll -155$ dBc/Hz for 1 mA of photocurrent. For phase-noise measurements using the phase detector method (the preferred technique), the system noise floor must be $\ll -161$ dBc/Hz for 1 mA of photocurrent. We have described techniques that will achieve this level of performance with currently available technology.

We have used our noise measurement system to characterize the amplitude noise of argon-ion and DPSS pump lasers as well as the amplitude and phase noise of a mode-locked femtosecond Ti:sapphire laser using both pumps. Strong correlation was observed between the AM noise spectra of the pump lasers and the phase-noise spectra of the Ti:sapphire laser.

ACKNOWLEDGMENT

The authors are especially grateful to R. Temple and T. Faulkner for sharing their expertise and patience on this interesting topic and to C. Bennett for early contributions.

REFERENCES

- [1] D. B. Sullivan, D. W. Allan, D. A. Howe, and F. L. Walls, Eds., *Characterization of Clocks and Oscillators: NIST Technical Note 1337*. Washington, DC: U.S. GPO, 1990.

[2] V. F. Kroupa, Ed., *Frequency Stability: Fundamentals and Measurement*. New York: IEEE Press, 1983.

[3] Hewlett-Packard Company, "Phase noise characterization of microwave oscillators: Phase detector method," Palo Alto, CA, Product Note 11729B-1, 1984.

[4] W. P. Robins, *Phase Noise in Signal Sources*. New York: Peter Peregrinus, 1982.

[5] G. K. Montress, T. E. Parker, and M. J. Loboda, "Residual phase noise measurements of VHF, UHF, and microwave components," in *Proc. 43rd Annu. Symp. Frequency Control*, 1989, pp. 349–359.

[6] D. von der Linde, "Characterization of the noise in continuously operating mode-locked lasers," *Appl. Phys. B*, vol. 39, pp. 201–217, 1986.

[7] M. J. W. Rodwell, K. J. Weingarten, D. M. Bloom, T. Baer, and B. H. Kolner, "Reduction of timing fluctuations in a mode-locked Nd:YAG laser by electronic feedback," *Opt. Lett.*, vol. 11, pp. 638–640, Oct. 1986.

[8] A. Finch, X. Zhu, P. N. Kean, and W. Sibbett, "Noise characterization of mode-locked color-center laser sources," *IEEE J. Quantum Electron.*, vol. 26, pp. 1115–1123, June 1990.

[9] T. J. Kane, "Intensity noise in diode-pumped single-frequency Nd:YAG lasers and its control by electronic feedback," *IEEE Photon. Technol. Lett.*, vol. 2, pp. 244–245, Apr. 1990.

[10] S. Sanders, T. Schrans, A. Yariv, J. Paslaski, J. E. Ungar, and H. A. Zarem, "Timing jitter and energy fluctuations in passively mode-locked two-section quantum-well laser coupled to an external cavity," *Appl. Phys. Lett.*, vol. 59, pp. 1275–1277, Sept. 1991.

[11] D. J. Derickson, P. A. Morton, J. E. Bowers, and R. L. Thornton, "Comparison of timing jitter in external and monolithic cavity mode-locked semiconductor lasers," *Appl. Phys. Lett.*, vol. 59, pp. 3372–3374, Dec. 1991.

[12] D. Henderson and A. G. Roddie, "A comparison of spectral and temporal techniques for the measurement of timing jitter and their application in a modelocked argon ion and dye laser system," *Opt. Commun.*, vol. 100, pp. 456–460, July 1993.

[13] I. G. Fuss, "An interpretation of the spectral measurement of optical pulse train noise," *IEEE J. Quantum Electron.*, vol. 30, pp. 2707–2710, Nov. 1994.

[14] S. Taccheo, P. Laporta, and O. Svelto, "Intensity noise reduction in a single-frequency ytterbium-codoped erbium laser," *Opt. Lett.*, vol. 21, pp. 1747–1749, Nov. 1996.

[15] M. Bisi and F. Bertinetto, "Amplitude noise and linewidth reduction of an Ar⁺ laser," *IEEE Trans. Instrum. Meas.*, vol. 46, pp. 153–155, Apr. 1997.

[16] M. Aoyama and K. Yamakawa, "Noise characterization of an all-solid-state mirror-dispersion-controlled 10-fs Ti:sapphire laser," *Opt. Commun.*, vol. 140, pp. 255–258, Aug. 1997.

[17] H. Tsuchida, "Correlation between amplitude and phase noise in a mode-locked Cr:LiSAF laser," *Opt. Lett.*, vol. 23, pp. 1686–1688, Nov. 1998.

[18] —, "Wideband phase-noise measurement of mode-locked laser pulses by a demodulation technique," *Opt. Lett.*, vol. 23, pp. 286–288, Feb. 1998.

[19] D. Eliyahu and A. Yariv, "Noise in passively mode-locked lasers," *Electron. Lett.*, vol. 34, pp. 779–780, Apr. 1998.

[20] H. Shi, I. Nitta, G. Alphonse, J. Connolly, and P. J. Delfyett, "Timing jitter performance of multiwavelength modelocked semiconductor laser," *Electron. Lett.*, vol. 34, pp. 2250–2252, Nov. 1998.

[21] J.-M. Shieh, S.-C. Liu, and C.-L. Pan, "Characterization and reduction of phase noise in passively mode-locked Ti:sapphire lasers with intracavity saturable absorbers," *J. Opt. Soc. Amer. B*, vol. 15, pp. 1802–1807, June 1998.

[22] T. R. Clark, T. F. Carruthers, P. J. Matthews, and I. N. D. III, "Phase noise measurements of ultrastable 10GHz harmonically modelocked fiber laser," *Electron. Lett.*, vol. 35, pp. 720–721, Apr. 1999.

[23] H. Tsuchida, "Time-interval analysis of laser-pulse-timing fluctuations," *Opt. Lett.*, vol. 24, pp. 1434–1436, Oct. 1999.

[24] H. Nagai, M. Kume, A. Yoshikawa, and K. Itoh, "Noise characterization of a Nd:YVO₄ laser pumped by laser diode modulated at high frequency," *Appl. Opt.*, vol. 33, pp. 5542–5545, Aug. 1994.

[25] H. A. Haus and A. Mecozzi, "Noise of mode-locked lasers," *IEEE J. Quantum Electron.*, vol. 29, pp. 983–996, Mar. 1993.

[26] L.-P. Chen, Y. Wang, and J.-M. Liu, "Spectral measurement of the noise in continuous-wave mode-locked laser pulses," *IEEE J. Quantum Electron.*, vol. 32, pp. 1817–1825, Oct. 1996.

[27] D. Eliyahu, R. Salvatore, and A. Yariv, "Noise characterization of a pulse train generated by actively mode-locked lasers," *J. Opt. Soc. Amer. B*, vol. 13, pp. 1619–1626, July 1996.

[28] —, "Effect of noise on the power spectrum of passively mode-locked lasers," *J. Opt. Soc. Amer. B*, vol. 14, pp. 167–174, Jan. 1997.

[29] F. G. Stremmer, *Introduction to Communication Systems*. Reading, MA: Addison-Wesley, 1977.

[30] Hewlett-Packard Co., "HP 3047A/11740A Phase Noise Measurement System," Palo Alto, CA, Feb. 1985.

[31] D. Allan *et al.*, "Standard terminology for fundamental frequency and time metrology," in *Proc. 42nd Ann. Frequency Control Symp. 1988*. New York: IEEE Press, June 1988, pp. 419–425.

[32] R. H. Kingston, *Optical Sources, Detectors, and Systems*. San Diego, CA: Academic, 1995.

[33] *Burr-Brown IC Applications Handbook*. Tucson, AZ: Burr-Brown Corporation, 1994.

[34] R. R. Hayes and D. L. Persechini, "Nonlinearity of p-i-n photodetectors," *IEEE Photon. Technol. Lett.*, vol. 5, pp. 70–72, Jan. 1993.

[35] K. J. Williams and R. D. Esman, "Photodiode dc and microwave nonlinearity at high current due to carrier recombination nonlinearities," *IEEE Photon. Technol. Lett.*, vol. 10, pp. 1015–1017, July 1998.

[36] H. Jiang, D. S. Shin, G. L. Li, T. A. Vang, D. C. Scott, and P. K. L. Yu, "The frequency behavior of the third-order intercept point in a waveguide photodiode," *IEEE Photon. Technol. Lett.*, vol. 12, pp. 540–542, May 2000.

[37] L. Lin *et al.*, "Velocity-matched distributed photodetectors with high-saturation power and large bandwidth," *IEEE Photon. Technol. Lett.*, vol. 8, pp. 1376–1378, Oct. 1996.

[38] H. W. Ott, *Noise Reduction Techniques in Electronic Systems*. John Wiley and Sons, 1976.

[39] H. Tsuchida, "Pulse timing stabilization of a mode-locked Cr:LiSAF laser," *Opt. Lett.*, vol. 24, pp. 1641–1643, Nov. 1999.

[40] F. M. Gardner, *Phaselock Techniques*, 2nd ed. New York: Wiley, 1979.



Ryan P. Scott (S'93) received the B.S. degree in laser electrooptics technology from Oregon Institute of Technology, Klamath Falls, in 1991 and the M.S. degree in electrical engineering from the University of California, Los Angeles (UCLA), in 1995, where he is currently pursuing the Ph.D. degree in electrical engineering.

In 1991, he joined the Laser Electro-Optic Research Group at UCLA, which moved to UC Davis. His current research work includes temporal imaging and precise measurement of laser amplitude

and phase noise.



Carsten Langrock received the Diploma in physics from the Heinrich-Heine-Universität, Düsseldorf, in 2001. He is currently pursuing the Ph.D. degree in electrical engineering at Stanford University, Stanford, CA.

Currently, he is a Research Assistant in the Ginzton Laboratory at Stanford University. His research interests include generation and detection of ultrashort optical pulses, nonlinear optics, and terahertz spectroscopy.



Brian H. Kolner (S'79–M'85) received the B.S. degree from the University of Wisconsin, Madison, in 1979 and the M.S. and Ph.D. degrees from Stanford University, Stanford, CA, in 1981 and 1985, respectively, all in electrical engineering.

From 1985 to 1991, he was a Member of Technical Staff at Hewlett-Packard Laboratories, Palo Alto, CA, where he worked on high-speed electronic and optoelectronic devices and measurement techniques using ultrashort laser pulses. In 1991, he joined the Electrical Engineering Department, University of California, Los Angeles (UCLA), and became Vice Chairman for Undergraduate Affairs in 1993. At UCLA he taught courses in microwave measurements, Fourier optics, and quantum mechanics and conducted research in space-time duality and temporal imaging. He joined the University of California, Davis, in 1996, where he holds joint appointments in the Departments of Applied Science and Electrical and Computer Engineering and the Lawrence Livermore National Laboratory. He teaches laser physics, electromagnetic theory, and optics. His current research interests are in temporal imaging, laser phase and amplitude noise, precision clocks and oscillators, and terahertz spectroscopy.

Dr. Kolner is a member of the Optical Society of America. He received a David and Lucile Packard Foundation Fellowship in 1991. He was a Guest Editor for the IEEE JOURNAL OF SPECIAL TOPICS IN QUANTUM ELECTRONICS in 1996.